Journal of Catalysis **188,** 403–412 (1999)
Article ID jcat.1999.2673, available online at http://www.idealibrary.com on IDEAL®

The Shape Selectivity of Paraffin Hydroconversion on TON-, MTT-, and AEL-Type Sieves

Th. L. M. Maesen,*,‡,[1] M. Schenk,† T. J. H. Vlugt,† J. P. de Jonge,‡ and B. Smit†

*Zeolyst International, PQ R and D Center, Conshohocken, Pennsylvania 19428-2240; †Department of Chemical Engineering, University of Amsterdam, Nieuwe Achtergracht 166, 1018 WV Amsterdam, The Netherlands; and ‡Shell Research and Technology Center, Shell International Chemicals, Amsterdam, The Netherlands

Received June 18, 1999; revised August 25, 1999; accepted August 27, 1999

Based on a comparison between simulated and measured adsorption properties, we demonstrate that both normal and monomethylparaffins are able to fully enter the pores of TON-, MTT-, and AEL-type molecular sieves. This disproves the theory that monomethylparaffins only partially enter these pores and that normal paraffins are predominantly hydroisomerized at the pore mouths of these sieves. Instead, we attribute the high selectivity for paraffins with terminal methyl groups to product shape selectivity, and the low selectivity for paraffins with neighboring methyl groups to transition state selectivity. These traditional shape selectivity concepts explain not only the detailed product distribution of *n*-heptane hydroconversion, but also that of longer-chain *n*-paraffins.

Key Words: **molecular simulations; paraffin hydroisomerization; zeolites; shape selectivity; pore mouth catalysis.**

INTRODUCTION

Molecular-sieve-based catalysts are widely used in many areas of the oil and petrochemical industries, because of their ability to catalyze reactions shape selectively (1). A recent example of the use of molecular sieves is the catalytic upgrading of lubricating oil (1). Noble metal loaded AEL-type silicoaluminophosphate molecular sieves selectively absorb the wax-like, long-chain normal paraffins from an oil feedstock and hydroconvert them selectively into branched paraffins (1–3). Catalysts based on TON- (4–7) and MTT-type (1, 4, 7–9) zeolites combine a strong affinity for long-chain, normal paraffins with a significantly higher selectivity for hydroisomerization than for hydrocracking (1–9).

Examination of the product slates reveals that when hydroisomerizing normal paraffins, TON-, MTT-, and AEL-type sieves preferentially introduce the first methyl group at a terminal position (3–7, 10, 11). Subsequent methyl groups are introduced at positions two or more methylene (viz. $-CH_2-$) groups removed from the ones already present (3–7, 12, 13). Since paraffins with methyl groups separated by fewer than two methylene groups are more susceptible to hydrocracking (6, 10), suppressing their formation automatically reduces the extent of hydrocracking. The selective adsorption and selective hydroconversion of the long-chain normal paraffins from a complex feedstock are characteristic of the 0.4- to 0.6-nm channel size (14) of the AEL-, TON-, and MTT-type molecular sieves. The selective adsorption clearly constitutes an example of reactant shape selectivity (RS, Fig. 1) (1, 15, 16). Less clear is how the preferential hydroisomerization relates to the shape selectivity imparted by the tubular one-dimensional AEL-, TON-, and MTT-type channels (14).

Current theories attribute the peculiar hydroisomerization pattern of AEL-, TON-, and MTT-type molecular sieves to either (i) pore mouth catalysis (PM) (6, 11–13), (ii) transition state shape selectivity (TS) (5, 7, 10, 17), or (iii) product shape selectivity (PS) (5, 18). The first theory postulates that the terminal branching occurs entirely at the pore mouths, because the required transition state does not fit inside a TON-type channel (6, 11–13). This theory has not been expanded to cover MTT- and AEL-type sieves. Since this model further postulates that none of the branched paraffins (11, 19) can fully enter the TON-type pores, it has to postulate that subsequent hydroisomerization reactions (to form di- and multibranched paraffins) occur at the pore mouths or at the external surface (6, 12, 13). The second theory suggests that the transition state required for terminal methyl groups is better able to fit inside the AEL-, TON-, and MTT-type channels than the transition state for internal methyl groups (5, 7, 17). Therefore, these channels would energetically favor the formation of the former. The third theory suggests a higher desorption rate for paraffins with terminal methyl groups than for paraffins with internal methyl groups (5, 18). The former therefore have shorter residence times and are less prone to consecutive reactions (PS) (5, 18).

To understand which of these theories is most accurate requires detailed information on the adsorption of the paraffins inside the molecular sieve pores. Information on a

[1] Current address: Zeolyst International, 280 Cedar Grove Road, PA 19428-2240. E-mail: tmaesen@pqcorp.com.

0021-9517/99 $30.00

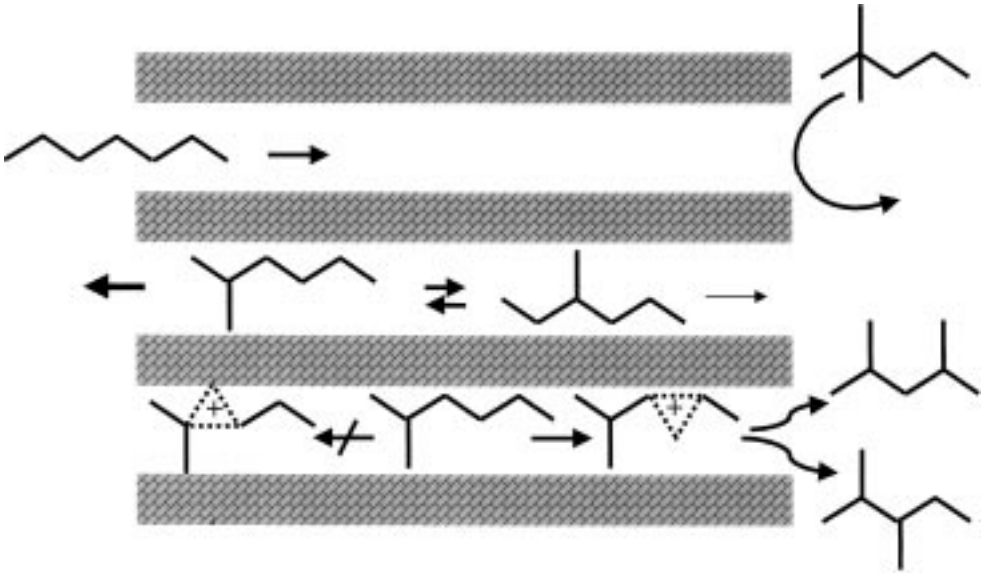

FIG. 1. Shape selectivity concepts (15, 16) valid for *n*-C_7 hydroconversion: (top) reactant selectivity (RS), (middle) product shape selectivity (PS), (bottom) transition state selectivity (TS).

molecular level can be obtained by complementing experimental adsorption data (19) with molecular simulations. Simulating the adsorption of long-chain or branched paraffins with conventional molecular simulation techniques would require excessive CPU time. The recently developed configurational-bias Monte Carlo (CBMC) technique circumvents this problem and allows calculation of the Henry coefficients and the adsorption enthalpies at zero coverage for paraffins in variously structured molecular sieves (20–22). The Henry coefficient quantifies the affinity of a particular hydrocarbon for a particular molecular sieve. For example, if the Henry coefficient of a molecule in a sieve is very low it is unlikely that such a molecule will adsorb in this sieve or that it will form as a reaction intermediate.

The linear and branched paraffins are modeled by considering the CH_3, CH_2, and CH groups as single interaction centers (united atoms). The bonded interactions include bond-bending and torsion potentials. The molecular sieve–paraffin interactions are assumed to be dominated by dispersive interactions with the oxygen atoms of the molecular sieve. The molecular sieve is modeled as a rigid crystal (23) so as to make the calculation of paraffin–sieve interactions efficient. This allows the use of special interpolation techniques (24, 25) to obtain the correct paraffin conformation at any given temperature. More details about the simulation method and the force fields are described elsewhere (26).

This paper compares the simulated sorption data with experimental sorption data available in the literature (19). The results of this comparison are then used to explain the differences between *n*-heptane (*n*-C_7) hydroconversion on TON-, MTT-, AEL-type sieves and FAU- or BEA-type zeolites. FAU- and BEA-type zeolites were chosen as a base case as their pores are too large to exert significant shape selectivity (27–31). Enough is known about the influence of the chain length on the hydroisomerization selectivity of *n*-paraffins (11, 32) to allow translation of the results for *n*-C_7 to the longer-chain paraffins that are more commonly described in the literature (4–7, 9–13, 17, 18).

EXPERIMENTAL METHODS

Catalyst Preparation

(a) TON-type zeolite (33). Aluminum sulfate hydrate (1.26 g) (Acros) was dissolved in a solution of 3.3 g sulfuric acid (Acros) in 33.4 g water. *N*-silicate (35.8 g) (PQ) was mixed into a solution of 0.22 g sodium hydroxide (Acros) in 44.7 g water. The sodium silicate was added to the aluminum sulfate solution, and the gel was homogenized. Subsequently 3.3 g of a 50 wt% sulfuric acid solution and 6.8 g diethylamine (DEA from Acros) were added. After thorough homogenization the gel (molar composition 90 SiO_2, 1 Al_2O_3, 50 DEA, 3 Na_2O, 24 Na_2SO_4, 3000 H_2O) was transferred to a Parr autoclave with a Teflon insert that was mounted onto a rotating wheel (14 rpm) inside an oven. After 48 h at 170°C a TON-type zeolite was harvested.

(b) MTT-type zeolite (34). First 1,3-diisopropylimidazolium chloride (henceforth called DPC) was made (35). Subsequently, 3.3 g NaOH (Acros) was dissolved in 97.3 g water, and 54.6 g of a 13.3 wt% solution of DPC in water was added followed by 55.2 g Ludox AS-30 (Dupont) and 35.0 g Nalco 1056. After stirring for 1 h at room temperature, the gel (molar composition 31 SiO_2, 1 Al_2O_3, 3 DPC, 3 Na_2O,

840 H_2O) was transferred to a Parr autoclave with a Teflon insert. After stirring (300 rpm) at 170°C for 95 h an MTT-type zeolite was isolated.

(c) AEL-type silicoaluminophosphate (36). Aluminum isopropoxide (20.43 g) (Acros) was added to 11.53 g of a 85 wt% H_3PO4 solution (Acros) in 31.57 g water. After stirring for 7 h at room temperature 1.28 g Ludox AS-40 (Dupont) and 5.06 g dipropylamine (DPA, Acros) were added, and the mixture was stirred for 16 h more. The resulting gel (molar composition 0.17 SiO_2, 1.0 Al_2O_3, 1.0 P_2O_5, 1.0 DPA, 70 H_2O) was transferred to an autoclave. After rotation (14 rpm) at 170°C for 30 h, an AEL-type silicoaluminophosphate was harvested.

(d) FAU- and BEA-type zeolites. FAU (unit cell size 2.430 nm, bulk Si/Al ratio 19 mol/mol, surface area 760 m^2/g)- and BEA-type (bulk Si/Al ratio 51 mol/mol, surface area 680 m^2/g) zeolites were provided by Zeolyst International.

Calcination for 6 h at 500°C removed the organic compounds from the TON-, MTT-, and AEL-type molecular sieves. Subsequently, these sieves were slurried three times with a 1.0 mol/L ammonium nitrate solution (10 ml per g of molecular sieve) at 80°C. All samples were loaded with 0.4 wt% Pt as verified by X-ray fluorescence. All zeolites were ion exchanged with platinum tetraamine hydroxide (Drijfhout) (37). The AEL-type silicoaluminophosphate was loaded by incipient wetness impregnation with platinum tetraamine hydroxide. Once loaded with a platinum salt, the sieves were calcined by a careful, staged calcination (37).

Analytical Techniques

We established that all sieves were free of crystalline impurities and that they were fully crystalline as determined by X-ray diffraction on a Phillips diffraction system equipped with a proportional solid state detector, using Cu$K\alpha$ radiation.

Elemental analyses were done using X-ray fluorescence (XRF) on a Philips X-unique wave dispersive spectrometer.

Nitrogen adsorption isotherms were recorded at 77 K on an ASAP 2000 apparatus (Micromeritics).

n-Heptane Hydrocracking Test

A fixed bed of a platinum-loaded powder (pressed and sieved into 30-80 mesh pellets) was activated by heating it to 400°C at 1°C/min in a H_2 flow rate of 14.9 ml/g/min (S.T.P.) and at 3 MPa total pressure. After 2 h at 400°C, the temperature of a zeolite sample was dropped to 350°C. Subsequently, a *n*-C_7 (Fluka) flow of 1.00 g/g/h was added to the H_2 flow. At the resultant total gram hourly space velocity (GHSV) of 1120 ml/g/h (S.T.P.) at 3 MPa total pressure (H_2/*n*-$C_7 = 240$ mol/mol), the temperature was decreased to 150°C at a rate of 0.22°C/min while periodically taking a sample for gas chromatographic analysis. For the AEL-type silicoaluminophosphate a temperature range from 400 to 200°C was scanned. For all sieves, activation energies were determined from 0 to 75 wt% conversion using first order kinetics. Above 70–75 wt% conversion first-order kinetics are no longer valid because formation of *n*-heptane from isoheptane becomes significant.

CBMC Calculations

The sizes of the molecules and the energy parameters have been fitted to the adsorption enthalpies and the Henry coefficients of linear and mono-branched paraffins in aluminum-free MFI-type silicates (26). The resultant force field reproduces the Henry coefficients, adsorption enthalpies and isotherms for linear and mono-branched paraffins up to a carbon number of 10. We assume that we can use the same force field for topologies other than MFI. The calculation of the Henry coefficient and the adsorption enthalpy at zero coverage requires two simulations in the NVT ensemble; one simulation of a paraffin in the presence of a zeolite and the other simulation in the ideal gas situation (26). In these simulations, there are three different trial moves:

(i) Displacement of a chain: a chain is selected at random and given a random displacement. The maximum displacement was taken such that 50% of the moves were accepted.

(ii) Rotation of a chain: a chain is selected at random and given a random rotation around the center of mass. The maximum rotation was selected such that 50% of the moves were accepted.

(iii) Regrowing of a chain: a chain is selected at random and is completely regrown at a randomly selected position. During this step data are collected from which the Henry coefficient is determined.

The relative probabilities for attempting these moves were such that 10% of the total number of moves were displacements, 10% rotations, and 80% regrowths of the entire molecule. A typical simulation consists of 2×10^6 Monte Carlo steps.

RESULTS AND DISCUSSION

To establish which paraffins are able to fit inside the pores of AEL-, TON-, and MTT-type sieves, we compare the adsorption enthalpies and Henry coefficients calculated by the CBMC technique with those measured (19) on a TON-type zeolite (Tables 1 and 2). The correlation between calculated and measured Henry coefficients of all the paraffins is excellent (Fig. 2, correlation coefficient $R^2 = 0.995$), and so is the correlation between the calculated and measured adsorption enthalpies of the linear paraffins (Fig. 3, $R^2 = 0.995$). The adsorption enthalpies calculated for the branched paraffins are consistently 7 kJ/mol lower than the

TABLE 1

Measured (19) and Calculated Adsorption Enthalpies (kJ/mol)

Name	Measured TON	Calculated TON	Calculated MTT	Calculated AEL
Pentane	−62.1	−62.0	−55.1	−60.5
2MeBut	−50.4	−59.8	−47.9	−57.4
Hexane	−75.0	−74.5	−67.1	−70.6
2MePen	−62.4	−69.9	−54.3	−71.5
3MePen	−61.7	−69.9	−54.1	−63.6
22diMeBut	−38.2	11.8	−45.9	−10.1
23diMeBut	−52.2	−60.6	−51.5	−61.1
Heptane	−87.9	−85.9	−76.3	−81.9
2MeHex	−75.4	−84.6	−69.7	−81.4
3MeHex	−69.8	−81.4	−66.2	−78.5
23diMePen	−60.2	−73.8	−46.0	−71.6
33diMePen		6.3	−55.5	−15.2

measured ones (Fig. 3, $R^2 = 0.95$), suggesting a systematic error in the force field. This could be the result of optimizing the force field for adsorption in a MFI-type framework, and not a TON-type. Moreover, the simulations assume a TON-type pure silicate, whereas the experimental TON-type sample is a zeolite containing protons and framework aluminum. Despite these differences, the simulations are in good agreement with the experimental data.

The CBMC technique simulates adsorption inside perfect, infinitely long, TON-type channels. Therefore the good agreement between the experimental and the simulated adsorption data for normal and monobranched paraffins implies that crystal imperfections or crystal boundaries did not significantly affect the experimental (19) data and that the *n*-C_7 and monobranched heptanes (i-C_7) are fully adsorbed inside the TON-type channels. The dibranched heptanes (henceforth referred to as ii-C_7) merit a more detailed evaluation.

TABLE 2

Measured (19) and Calculated Henry Coefficients (μmol/kg Pa)

Name	Measured TON	Calculated TON	Calculated MTT	Calculated AEL
Pentane	1.32E + 00	6.45E − 01	3.92E − 02	4.14E − 01
2MeBut	3.23E − 01	1.23E − 01	3.37E − 03	1.07E − 01
Hexane	2.59E + 00	1.43E + 00	7.84E − 02	6.80E − 01
2MePen	5.42E − 01	2.28E − 01	3.88E − 03	4.71E − 01
3MePen	4.42E − 01	1.76E − 01	6.93E − 04	6.39E − 02
22diMeBut	1.30E − 01	1.80E − 09	1.52E − 04	1.16E − 07
23diMeBut	2.39E − 01	7.42E − 03	2.01E − 04	9.86E − 03
Heptane	4.66E + 00	2.81E + 00	7.21E − 02	9.84E − 01
2MeHex	1.13E + 00	6.74E − 01	1.58E − 02	8.13E − 01
3MeHex	8.71E − 01	3.42E − 01	1.32E − 03	2.11E − 01
23diMePen	4.19E − 01	1.54E − 02	1.22E − 05	1.83E − 02
33diMePen		5.98E − 10	3.75E − 05	4.51E − 08

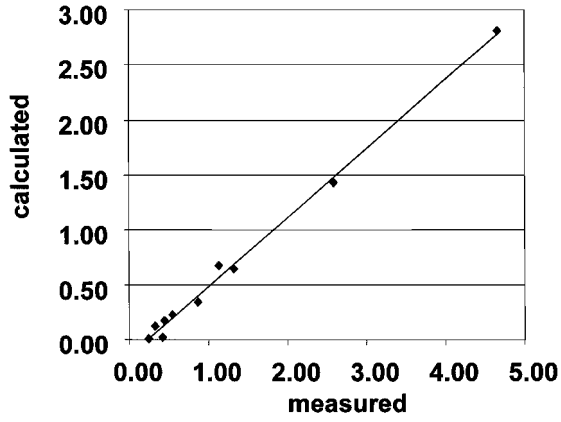

FIG. 2. Comparison of measured and calculated Henry coefficients (μmol/kg Pa) at 573 K: data (◆), and correlation (—).

The calculated adsorption enthalpies for dibranched paraffins with geminal methyl groups (such as 3,3-dimethylpentane and 2,2-dimethylbutane) are positive (Table 1) and the Henry coefficients approach zero μmol/kg Pa (Table 2), suggesting that the TON-type channels do not permit access to this type of paraffins. The experimentally determined Henry coefficient of 0.13 μmol/kg Pa for 2,2-dimethylbutane (Table 1) can be explained as resulting from adsorption outside the pores (at sample imperfections such as pore mouths and intercrystalline voids) (19).

The calculated Henry coefficients for dibranched paraffins with vicinal methyl groups (such as 2,3-dimethylpentane and 2,3-dimethylbutane), are slightly below the experimental values (Table 2). The calculated adsorption enthalpies compare well with the experimentally determined enthalpies of adsorption, and are not as prohibitively high as those of paraffins with geminal methyl groups (Table 1). It is tempting to conclude that the size of ii-C_7 molecules with vicinal methyl groups is at the limit of what can fit inside the TON-type pores. The same holds

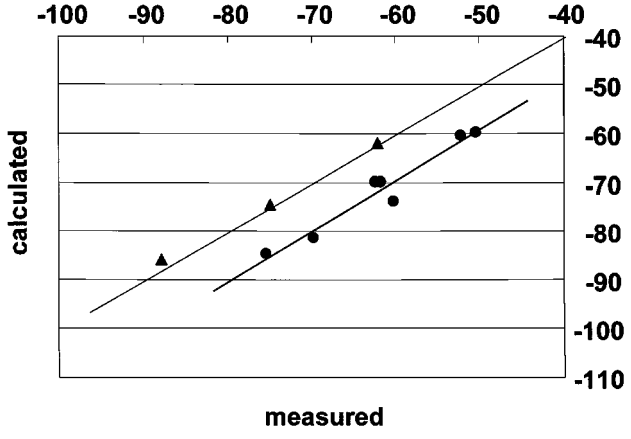

FIG. 3. Comparison of measured and calculated adsorption enthalpies (kJ/mol): (▲) linear paraffins, (●) branched paraffins.

TABLE 3

Molecular Sieve Pore Dimensions, Micropore Volume (micro pV) as Determined by Nitrogen Sorption, Temperature Required for 40% *n*-C_7 Hydroconversion ($T_{40\%}$ (K)), Maximum i-C_7 and ii-C_7 Yield (wt%), and Activation Energy E_{act} (kJ/mol)

Structure type	Max diameter (nm)	Min diameter (nm)	Micro pV (ml/g)	$T_{40\%}$ (K)	Max i-C_7 (wt%)	Max ii-C_7 (wt%)	E_{act} (kJ/mol)
FAU	0.74	0.74	0.24	510	50.1	24.4	134
BEA	0.76	0.55	0.21	492	51.7	21.7	138
TON	0.55	0.44	0.09	525	66.2	5.7	141
MTT	0.52	0.45	0.06	521	66.2	4.7	144
AEL	0.63	0.39	0.11	578	62.2	14.7	118

true for the slightly smaller ii-C_7 with methyl groups separated by one $-CH_2-$ group (quasi-vicinal methyl groups). The simulations, which employ a rigid framework, do not allow us to draw unambiguous conclusions about the adsorption of molecules whose size approaches that of the pore diameter. Additional conclusions about the constraints imposed by TON-, MTT-, and AEL-type channels on these types of ii-C_7 molecules can be derived from the results of the catalytic *n*-C_7 hydroconversion tests (see below).

In order to discuss the peculiarities of the shape selective *n*-C_7 hydroisomerization, it is useful to first address what happens in the absence of shape selectivity, using the nonselective *n*-C_7 hydroconversion on Pt-loaded FAU- and BEA-type zeolites as an example. Under the experimental conditions, the FAU- and BEA-type zeolites exhibit virtually identical selectivity (Table 3). The following model can be used to describe the hydroisomerization of *n*-C_7 into i-C_7, ii-C_7, and the subsequent hydrocracking of ii-C_7 to yield isobutane (i-C_4) and propane (C_3) (27–32) (Fig. 4):

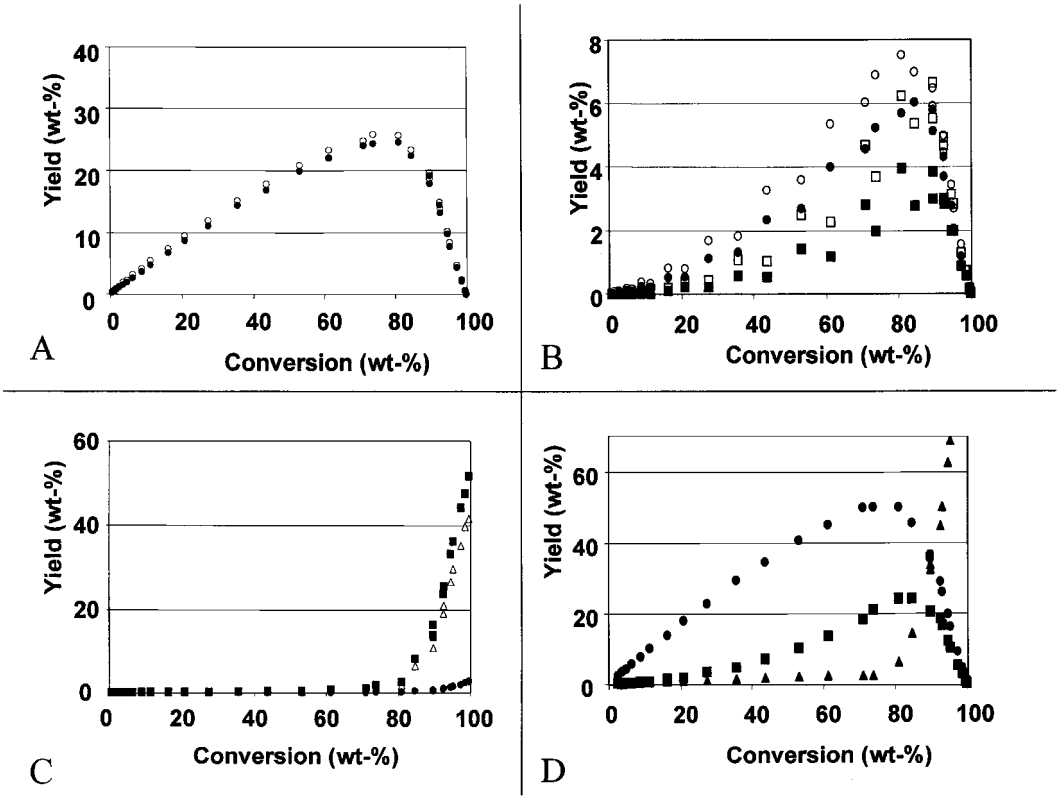

FIG. 4. (A) i-C_7 yield pattern on FAU- or BEA-type zeolite: (●) 2-methylhexane, (○) 3-methylhexane. (B) ii-C_7 yield pattern on FAU- or BEA-type zeolite: (●) 2,4-dimethylpentane, (○) 2,3-dimethylpentane, (■) 3,3-dimethylpentane, (□) 2,2-dimethylpentane. (C) *n*-C_7 hydrocracking pattern on FAU- or BEA-type zeolite: (△) propane, (■) iso-butane, (●) *n*-butane. (D) *n*-C_7 hydroconversion pattern on FAU- or BEA-type zeolite: (●) i-C_7, (■) ii-C_7, (▲) $C_4 + C_3$.

$$n\text{-}C_7 \rightleftarrows \text{i-}C_7 \rightleftarrows \text{ii-}C_7 \rightarrow \text{i-}C_4 + C_3.$$

Since the yield of 2,2,3-trimethylbutane remains below 1.5 wt%, it is not included in the discussion. As observed elsewhere (27), FAU- and BEA-type zeolites yield the two i-C_7 molecules (2- and 3-methylhexane) at thermodynamic equilibrium (Fig. 4A). The kinetically favored 2,3-dimethylpentane (29) and thermodynamically favored 2,4-dimethylpentane (29) dominate the ii-C_7 yield (Fig. 4B). The approximately equal yield of i-C_4 and of C_3 (Fig. 4C) indicates (29) that FAU- and BEA-type zeolites predominantly hydrocrack ii-C_7 as opposed to i-C_7. The methane and ethane yields of the FAU- and BEA-type zeolites remain below 0.1 wt% (at 98% conversion), indicating that the Pt phase is sufficiently active to establish an equilibrium between the adsorbed paraffins and the olefins and that Pt-catalyzed cracking (28–30) and hydroisomerization (38, 39) are negligible. The catalysts based on TON-, MTT-, and AEL-type sieves have a slightly higher Pt-catalyzed hydroconversion (combined methane and ethane yield 4 wt% at 98% conversion).

The n-C_7 hydroconversion selectivity of TON- and MTT-type zeolites (Fig. 5) is markedly different from that of FAU- or BEA-type zeolites (Fig. 4). Notwithstanding the difference in pore shape (14, 33) and sorption properties (Tables 1 and 2) between the TON- and the MTT-type zeolites, their n-C_7 hydroconversion selectivity is comparable (Table 3). Both yield a ratio of terminal i-C_7 (viz. 2-methylhexane) to internal i-C_7 (viz. 3-methylhexane) in excess of thermodynamic equilibrium (Fig. 5A), whereas FAU- and BEA-type zeolites yield i-C_7 at equilibrium. As discussed above, current theories explain this high selectivity for terminal methyl groups in terms of either (i) pore mouth catalysis (PM), (ii) transition state selectivity (TS), or (iii) product selectivity (PS).

Pore mouth catalysis (PM) was born when molecular graphics calculations suggested that neither the transition state, nor a branched paraffin, would fit inside the TON-type pores (11). Therefore it was postulated that hydroisomerization favors the formation of a terminal methyl group because hydroisomerization occurs exclusively at the supposedly enlarged (6, 12) TON-type pore mouths. Recent evaluations (40, 41) of the transition state for paraffin hydroisomerization show that the size of the transition state in the original molecular graphics calculations (11, 42) was overestimated. According to this recent assessment (40, 41), the transition state for forming i-C_7 (a corner-protonated 1-methyl, 2-propyl-, or 1,2-diethylcyclopropyl cation (29))

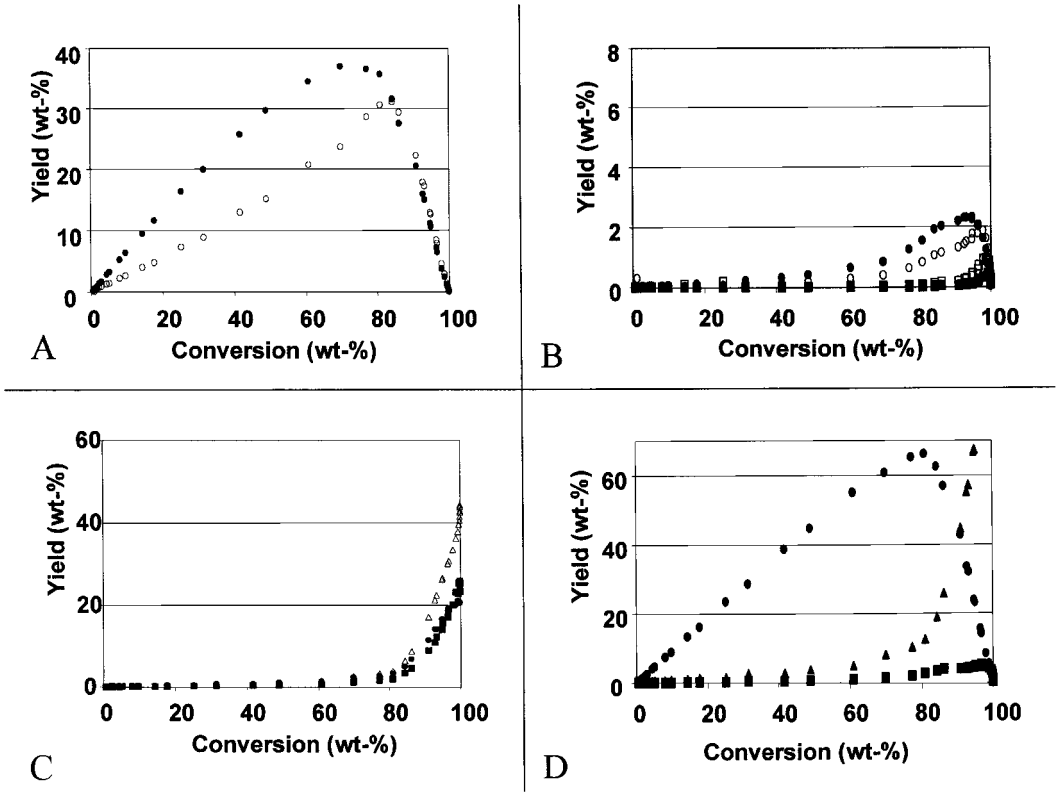

FIG. 5. (A) i-C_7 yield pattern on TON- or MTT-type zeolite: (●) 2-methylhexane, (○) 3-methylhexane. (B) ii-C_7 yield pattern on TON- or MTT-type zeolite: (●) 2,4-dimethylpentane, (○) 2,3-dimethylpentane, (■) 3,3-dimethylpentane, (□) 2,2-dimethylpentane. (C) n-C_7 hydrocracking pattern on TON- or MTT-type zeolite: (△) propane, (■) iso-butane, (●) n-butane. (D) n-C_7 hydroconversion pattern on TON- or MTT-type zeolite: (●) i-C_7, (■) ii-C_7, (▲) $C_4 + C_3$.

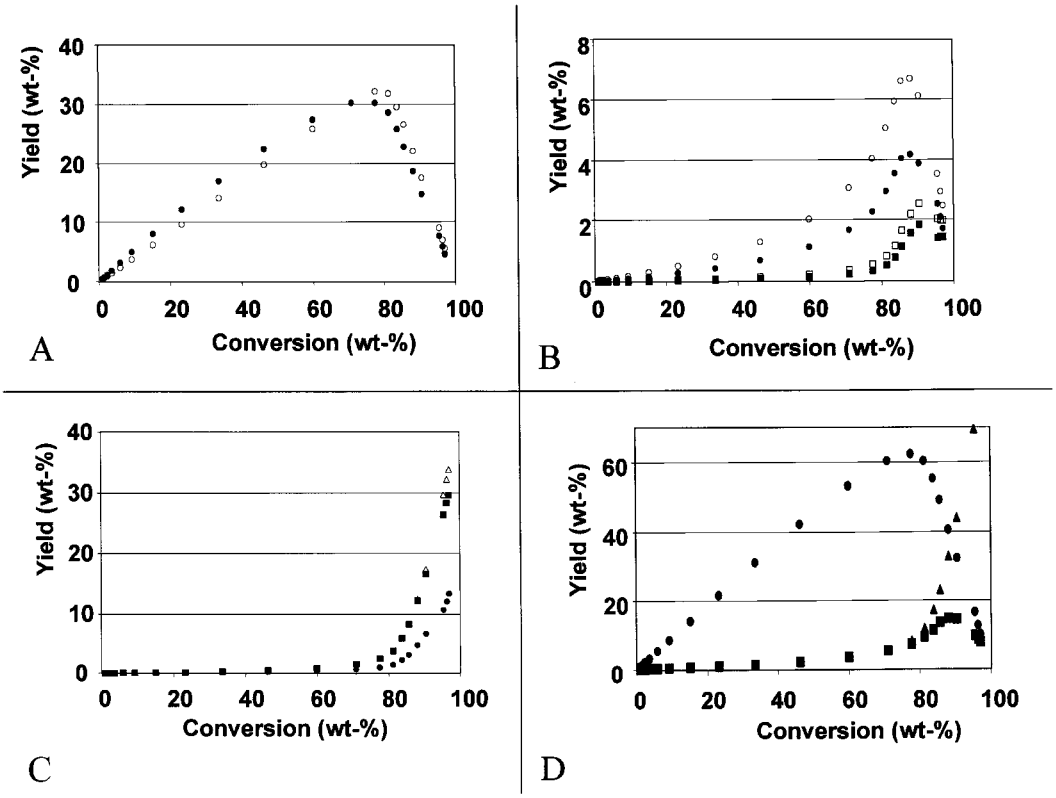

FIG. 6. (A) i-C_7 yield pattern on AEL-type sieve: (●) 2-methylhexane, (○) 3-methylhexane. (B) ii-C_7 yield pattern on AEL-type sieve: (●) 2,4-dimethylpentane, (○) 2,3-dimethylpentane, (■) 3,3-dimethylpentane, (□) 2,2-dimethylpentane. (C) *n*-C_7 hydrocracking pattern on AEL-type sieve: (△) propane, (■) iso-butane, (●) *n*-butane. (D) *n*-C_7 hydroconversion pattern on AEL-type sieve: (●) i-C_7, (■) ii-C_7, (▲) $C_4 + C_3$.

is smaller than i-C_7. Comparing experimental data with CBMC calculations, we have established that i-C_7 fits inside the TON-type pores. Since the transition state for i-C_7 is smaller than its i-C_7 product, it too should fit snugly inside the TON-type channels, and there is no reason for their preferential formation at the pore mouths. Thus the molecular graphics basis for postulating pore mouth catalysis appears not to have withstood the test of time. This leaves transition state (TS) and product selectivity (PS) as viable explanations for the enhanced selectivity for terminal methyl groups.

If the i-C_7 product distribution were dependent on the transition state for the hydroisomerization of *n*-C_7 into i-C_7, we would expect FAU- and BEA-type zeolites to yield predominantly the kinetically favored internal methyl groups (Fig. 7). This is not the case (Fig. 4A), because intramolecular methyl-shifts rapidly bring the i-C_7 molecules with terminal and with internal methyl groups to thermodynamic equilibrium (29). Since methyl-shifts appear to nullify the effect of the transition states in FAU- and BEA-type zeolites, transition state selectivity is unlikely to be the main explanation for the shape selective production of paraffins with terminal methyl groups by the TON- and MTT-type pores. Nonetheless, it cannot be ruled out entirely (7, 17) without a more careful study similar to that carried out for MFI-type zeolites (10). A more plausible explanation is that these pores contain equal amounts of paraffins with terminal and with internal methyl groups (the equilibrium distribution) and selectively release more of the former as they diffuse faster out of the pores (PS). Indeed, for several zeolites, the ratio of the selectivity for paraffins with a terminal methyl group to that for paraffins with an internal methyl group appears to correlate quite well with the ratio of the respective diffusion rate of these molecules out of the zeolite pores (18).

Not only the i-C_7 product slate, but also the ii-C_7 product slate of TON- and MTT-type zeolites is markedly different from that of FAU- and BEA-type zeolites (cf. Figs. 4B and 5B). The TON- and MTT-type zeolites yield no paraffins with geminal methyl groups and only few with (quasi-) vicinal methyl groups, preferentially yielding 2,4-dimethylpentane (Fig. 5B). This absence of geminal methyl groups confirms that the TON- and MTT-type channels exclude them. Pore mouth catalysis (PM) postulates that the TON-type structure absorbs monomethylparaffins at the outer crystal surface by pinning them down by a methyl group at a pore mouth (key–lock mechanism (6, 12, 13)). Subsequent hydroisomerization occurs at the active sites in

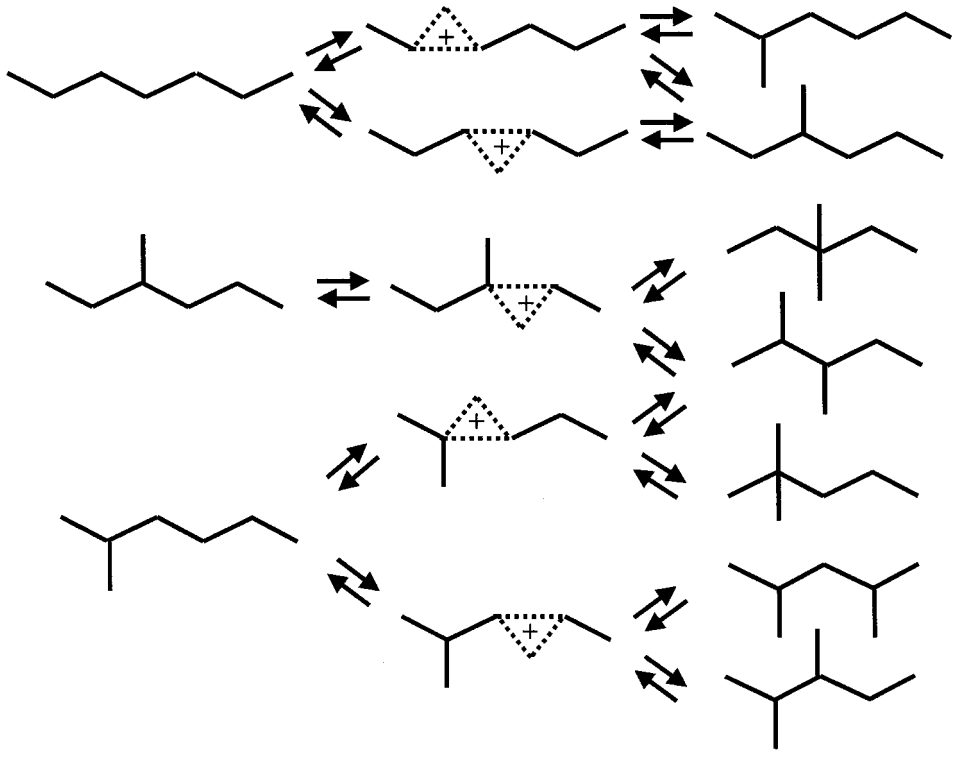

FIG. 7. Relevant reactants, transition states, and products of *n*-C_7 hydroconversion.

a neighboring pore mouth, and the position of the subsequent branches is governed by the position of the neighboring pore mouths (6, 12, 13). This model cannot explain the preferential formation of 2,4-dimethylpentane, because the i-C_7 chain is too short to bridge the space between neighboring pore mouths. As demonstrated above, the i-C_7 is able to enter the TON-type pores. Given its high adsorption enthalpy (Table 1) it will enter the pores and will not linger at or near the outer crystal surface. This leaves transition state (TS) and product selectivity (PS) as the only feasible options for explaining the shape selective formation of 2,4-dimethylpentane inside the TON- and MTT-type pores.

The size of the transition state for forming i-C_7 approaches that of i-C_7 (40, 41). By the same token we expect the size of the (corner-protonated) trialkyl cyclopropyl transition state for forming geminal methyl groups (Fig. 7) to approach the size of their products. Since the TON- and MTT-type pores exclude the products, they can reasonably be expected to exclude the transition states. The resulting inhibition leaves only the dialkyl cyclopropyl cation transition state for forming dimethylparaffins (Fig. 7). Having only one of three transition states available for forming ii-C_7 (Fig. 7) would explain the comparatively low yield of ii-C_7 (cf. Figs. 4B and 5B) (TS). When the dialkyl cyclopropyl cation transition state is the only route toward dimethylparaffins, it will initially yield equal amounts of 2,3- and 2,4-dimethylpentane (Fig. 7). The enhanced yield of the latter suggests that these ii-C_7 molecules reside long enough inside the TON- and MTT-type channels for methyl shifts to generate predominantly the thermodynamically favored, faster diffusing 2,4-dimethylpentane (29) (PS).

The shape selectivity of the TON- and MTT-type zeolites is also evident in their hydrocracking product slate (Fig. 5C). While FAU- or BEA-type zeolites predominantly yield C_3 and i-C_4 (Fig. 4C), the TON- and MTT-type product slates are complemented with significant quantities of *n*-butane (Fig. 5C). The presence of *n*-butane implies that these zeolites impede i-C_7 hydroisomerization to such an extent that the energetically less favorable i-C_7 hydrocracking becomes significant (29). The postulated inhibition of the formation of trialkyl cyclopropyl transition states impedes i-C_7 hydroisomerization, for it would require 3-methylhexane to methyl-shift into 2-methylhexane before it is able to hydroisomerize (Fig. 7). In addition, it would leave 2-methylhexane with access to only one instead of two transition states for hydroisomerization (Fig. 7). The remaining transition state for i-C_7 hydroisomerization is still quite bulky, for it contains a methyl group adjacent to the cyclopropyl cation (Fig. 7). We can easily envisage that the restricted space available inside the TON- and MTT-type channels increases the formation energy of such a bulky transition state to the extent that it approaches the activation energy for i-C_7 hydrocracking (TS). This would explain why an energetically unfavorable reaction such as

i-C_7 hydrocracking occurs concomitantly with i-C_7 hydroisomerization.

Having shown how the transition state and product shape selectivity affect the individual product slates we are now in a position to address the overall *n*-C_7 hydroisomerization reaction in the TON- and MTT-type zeolites (Fig. 5D). Compared with FAU- and BEA-type zeolites (Fig. 4D), the TON- and MTT-type zeolites yield more i-C_7, yield less ii-C_7, and start hydrocracking at a lower hydroconversion level (Fig. 5D). The enhanced i-C_7 selectivity and reduced ii-C_7 selectivity can be explained by the impediment of the consecutive hydroisomerization of i-C_7 into ii-C_7 (TS). The onset of hydrocracking at lower conversion can be attributed to branched paraffins being constrained inside the tubular TON- and MTT-type channels. The increased intracrystalline residence time (as compared to FAU- or BEA-type zeolites) increases the chance of these molecules being hydrocracked (PS).

As may be predicted based on its intermediate pore size (Table 3) (14), the *n*-C_7 hydroconversion selectivity of the AEL-type silicoaluminophosphate lies somewhere in between that of the FAU- or BEA-type zeolites and the TON- or MTT-type zeolites. As with FAU- and BEA-type zeolites, the AEL-type sieve yields a product slate that is only marginally enhanced in i-C_7 molecules with terminal methyl groups (Fig. 6A), contains paraffins with geminal methyl groups, and is dominated by the kinetically favored 2,3-dimethylpentane (Fig. 6B). Like TON- and MTT-type zeolites, the AEL-type sieve has a high i-C_7 selectivity (Fig. 6D), has a low ii-C_7 selectivity (particularly for ii-C_7 molecules with geminal methyl groups, Fig. 6B), and hydrocracks i-C_7 (Fig. 6C) at relatively low conversion (Fig. 6D).

The concepts for explaining the hydroconversion of *n*-C_7 on TON-, MTT-, and AEL-type sieves can also be used to explain the hydroconversion of longer-chain paraffins like *n*-C_{12} (4), *n*-C_{16} (3), and *n*-C_{17} (6). When converting longer-chain paraffins, these particular sieves enhance not only the selectivity for monobranched but also that for dibranched paraffins, and they suppress hydrocracking (3–7, 9–12, 17). The methyl groups in the dibranched paraffins are at least two methylene groups apart, preferably even further (3, 4, 6, 9, 12, 13). Analogous to i-C_7, transition state selectivity would explain the inhibition of geminal methyl groups and the absence of quasi-vicinal methyl groups. The selectivity for the individual noninhibited dimethylparaffins will be dominated by their relative diffusion rate (PS). Unlike i-C_7, the initial methyl group need not affect the consecutive hydroisomerization as long as the second methyl group is introduced far enough away (TS). In the absence of geminal or quasi-vicinal methyl groups hydrocracking is more difficult than hydroisomerization (6, 10) (TS), so that both primary and consecutive hydroisomerization can continue until very high *n*-paraffin conversions are reached (3, 4, 6, 12, 13). Thus, we can explain the phenomena normally used to illustrate pore mouth catalysis concepts (6, 12, 13) by traditional shape selectivity concepts.

Finally, the activation energy of a reaction can be used to assess whether the complete pore or only the pore mouth is involved in paraffin hydroconversion. If the reaction is diffusion limited, the *n*-paraffin hydroconversion will be limited to the pore mouth. Diffusion limitations will lower the apparent activation energy for *n*-C_7 hydroconversion when the prerequisites for a diffusional increase in apparent activation energy are not met (43–45), as is the case with TON-, MTT-, and AEL-type sieves. We find that the apparent activation energies for the FAU-, BEA-, TON-, and MTT-type zeolites are comparable (Table 3, estimated systematic error ± 3 kJ/mol) and approach the true activation energy for hydroisomerization (43, 46, 47). This indicates that there are no diffusion limitations and therefore all of the zeolite acid sites are able to contribute to the *n*-C_7 hydroconversion (43, 46, 47), leaving little room for speculation that the *n*-C_7 hydroconversion in the TON- or MTT-type zeolites occurs predominantly at or near the pore mouth. The apparent activation energy of the AEL-type silicoaluminophosphate is lower than that of the zeolites (Table 3), indicating either a lower acid site coverage (due to its higher operation temperature (Table 3)) or the onset of diffusion limitations (43, 45). Determining which is the case would require determining the acid site coverage.

CONCLUSIONS

The good fit between measured and simulated adsorption constants (Henry coefficients and adsorption enthalpies) establishes that normal paraffins with only one methyl group are able to enter the TON-, MTT-, and AEL-type pores, and that paraffins with geminal methyl groups are not. The shape selective formation of paraffins with (quasi-) vicinal methyl groups indicates that these, too, are able to enter the TON-, MTT-, and AEL-type pores, albeit with difficulty. Thanks to this evaluation of the molecular sizes, we are able to rule out that paraffins with one methyl group are predominantly hydroisomerized at the pore mouths. An analysis of the activation energy corroborates this finding. Instead, we can explain the high selectivity of the TON-, MTT-, and AEL-type sieves for paraffins with terminal methyl groups in terms of product selectivity and the low selectivity for paraffins with proximate methyl groups in terms of transition state selectivity (Fig. 1). An unambiguous evaluation of pore mouth catalysis would require studying molecular sieves that clearly absorb linear paraffins but exclude all branched paraffins.

ACKNOWLEDGMENTS

The authors thank W. H. J. Stork for fruitful discussions, I. M. van Vegchel, C. M. van Ballegoy, W. G. M. Hoogervorst, W. Kant, and

C. Engelen for assistance with the sample preparation and J. van Mechelen for help with the X-ray diffraction and C. H. Roemkens for comments on the manuscript. T.J.H.V. thanks the NWO-CW (Nederlandse Organisatie voor Wetenschappelijk Onderzoek, Chemische Wetenschappen) for financial support, B.S. the OSPT. SARA (Stichting Academisch Rekencentrum Amsterdam) generously provided a large part of the computer resources. We acknowledge additional support by the Organization for Scientific Research in the Netherlands (NWO) through PIONIER.

REFERENCES

1. Maxwell, I. E., and Stork, W. H. J., *in* "Introduction to Zeolite Science and Practice" (H. van Bekkum, E. M. Flanigen, and J. C. Jansen, Eds.), Vol. 58, pp. 571–630. Elsevier, Amsterdam, 1991.
2. Miller, S. J., *in* "Zeolites and Related Microporous Materials: State of the Art 1994" (J. Weitkamp, H. G. Karge, H. Pfeifer, and W. Hölderich, Eds.), Vol. 84, pp. 2319–2326. Elsevier, Amsterdam, 1994.
3. Miller, S. J., *Microporous Mater.* **2**, 439–449 (1994).
4. Ernst, S., Kokotailo, G. T., Kumar, R., and Weitkamp, J., *in* "Proceedings, 9th International Congress on Catalysis, Calgary 1988" (M. J. Phillips and M. Ternan, Eds.), Vol. 1, pp. 388–395. Chem. Institute of Canada, Ottawa, 1988.
5. Ernst, S., Weitkamp, J., Martens, J. A., and Jacobs, P. A., *Appl. Catal.* **48**, 137–148 (1989).
6. Souverijns, W., Martens, J. A., Froment, G. F., and Jacobs, P. A., *J. Catal.* **174**, 177–184 (1998).
7. Mériaudeau, P., Tuan, Vu. A., Sapaly, G., Nghiem, Vu. T., and Naccache, C., *in* "Proceedings of the 12th International Zeolite Conference" (M. M. J. Treacy, B. K. Marcus, M. E. Bisher, and J. B. Higgins, Eds.), Vol. IV, pp. 2913–2920. Materials Research Society, Warrendale, PA, 1999.
8. Bendoraitis, J. G., Chester, A. W., Dwyer, F. G., and Garwood, W. E., *in* "New Developments in Zeolite Science and Technology" (Y. Murakami, A. Lijima, and J. W. Ward, Eds.), Vol. 28, pp. 669–675. Elsevier, Amsterdam, 1986.
9. Ernst, S., Kumar, R., and Weitkamp, J., *Catal. Today* **3**, 1–10 (1988).
10. Martens, J. A., and Jacobs, P. A., *Zeolites* **6**, 334–348 (1986).
11. Martens, J. A., Parton, R., Uytterhoeven, L., Jacobs, P. A., and Froment, G. F., *Appl. Catal.* **76**, 95–116 (1991).
12. Martens, J. A., Souverijns, W., Verrelst, W., Parton, R., Froment, G. F., and Jacobs, P. A., *Angew. Chem. Int. Ed. Engl.* **34**(22), 2528–2530 (1995).
13. Souverijns, W., Martens, J. A., Uytterhoeven, L., Froment, G. F., and Jacobs, P. A., *in* "Progress in Zeolite and Microporous Materials" (H. Chon, S.-K. Ihm, and Y. S. Uh, Eds.), Vol. 105, pp. 1285–1292. Elsevier, Amsterdam, 1997.
14. Meier, W. M., Olson, D. H., and Baerlocher, Ch., "Atlas of Zeolite Structure Types," 4th ed., Elsevier, London, 1996.
15. Weisz, P. B., *Pure Appl. Chem.* **52**, 2091–2103 (1980).
16. Csicsery, S. M., *Zeolites* **4**, 202–213 (1984).
17. Mériaudeau, P., Tuan, Vu. A., Lefebvre, F., Nghiem, V. T., and Naccache, C., *Microporous Mesoporous Mater.* **22**, 435–449 (1998).
18. Webb III, E. B., and Grest, G. S., *Catal. Lett.* **56**, 95–104 (1998).
19. Denayer, J. F., Souverijns, W., Jacobs, P. A., Martens, J. A., and Baron, G. V., *J. Phys. Chem.* **102**, 4588–4597 (1998).
20. Siepmann, J. I., and Frenkel, D., *Mol. Phys.* **75**, 59–70 (1992).
21. Frenkel, D., Mooij, G. C. A. M., and Smit, B., *J. Phys. Condens. Matter.* **4**, 3053–3076 (1992).
22. de Pablo, J. J., Laso, M., and Suter, U. W., *J. Chem. Phys.* **967**, 6157–6162 (1992).
23. Bezus, A. G., Kiselev, A. V., Lopatkin, A. A., and Du, P. Q., *J. Chem. Soc. Faraday Trans. II* **74**, 367–379 (1978).
24. June, R. L., Bell, A. T., and Theodorou, D. N., *J. Phys. Chem.* **96**, 1051–1060 (1992).
25. Smit, B., and Siepmann, J. I., *J. Phys. Chem.* **98**, 8442–8452 (1994).
26. Vlugt, T. J. H., Krishna, R., and Smit, B., *J. Phys. Chem. B* **103**, 1102–1118 (1999).
27. Froment, G. F., *Catal. Today* **1**, 455–473 (1987).
28. Froment, G. F., *in* "Hydrotreatment and Hydrocracking of Oil Fractions" (G. F. Froment, B. Delmon, and P. Grange, Eds.), Vol. 106, p. 379. Elsevier, Amsterdam, 1997.
29. Gianetto, G. E., Perot, G. R., and Guisnet, M. R., *Ind. Eng. Chem. Prod. Res. Dev.* **25**, 481–490 (1986).
30. Degnan, T. F., and Kennedy, C. R., *AIChE J.* **39**(4), 607–614 (1993).
31. Blomsma, E., Martens, J. A., and Jacobs, P. A., *J. Catal.* **165**, 241–248 (1997).
32. Weitkamp, J., *in* "Hydrocracking and Hydrotreating," ACS Symposium Series, Vol. 20, pp. 1–27. Am. Chem. Soc., Washington, DC, 1975.
33. Jacobs, P. A., and Martens, J. A., "Synthesis of High-Silica Aluminosilicate Zeolites" (B. Delmon and J. T. Yates, Eds.), Vol. 33. Elsevier, Amsterdam, 1987.
34. Zones, S. I., Ziemer, J. N., Santilli, D. S., Innes, R. A., and Holterman, D. L., U.S. 5300210, 1993.
35. Arduengo, A. J., WO patent 91/14678.
36. Lok, B. M., Messina, C. A., Patton, R. L., Gajek, R. T., Cannan, Th. R., and Flanigen, E. M., US patent 400438, 1982.
37. Kouwenhoven, H. W., and van Helden, H. J. A., Ger. Offen. 1816822, 1969.
38. Chow, M., and McVicker, G. B., *J. Catal.* **112**, 303–312 (1988).
39. Blomsma, E., Martens, J. A., and Jacobs, P. A., *in* "Progress in Zeolite and Microporous Materials" (Y. Chon, S.-K. Ihm, and Y. S. Uh, Eds.), Vol. 105, pp. 909–916. Elsevier, Amsterdam, 1997.
40. Frash, M. V., Kazansky, V. B., Rigby, A. M., and van Santen, R. A., *J. Phys. Chem. B* **101**, 5346–5351 (1997).
41. Natal-Santiago, M. A., Alcalá, R., and Dumesic, J. A., *J. Catal.* **181**, 124–144 (1999).
42. Radom, L., Hariharan, P. C., Pople, J. A., and Schleyer, P. v. R., *J. Am. Chem. Soc.* **95**, 6531–6544 (1973).
43. van de Runstraat, A., van Grondelle, J., and van Santen, R. A., *J. Catal.* **167**, 460–463 (1997).
44. Rödenbeck, Ch., Kärger, J., and Hahn, K., *J. Catal.* **176**, 513–526 (1998).
45. Rödenbeck, Ch., Kärger, J., Hahn, K., and Sachtler, W., *J. Catal.* **183**, 409–410 (1999).
46. van de Runstraat, A., van Grondelle, J., and van Santen, R. A., *Ind. Eng. Chem. Res.* **36**, 3116–3125 (1997).
47. van de Runstraat, A., Kamp, J. A., Stobbelaar, P. J., van Grondelle, J., Krijnen, S., and van Santen, R. A., *J. Catal.* **171**, 77–84 (1997).